

Chapter 3

Whispering Gallery Mode Resonators as Biosensors

The previous chapter introduces biosensor technologies according to the physical nature of their signal transduction processes. Optical biosensors are just one category that includes a wide array of novel devices. The present work deals with a technology based on whispering gallery mode (WGM) optical resonators [60, 61]. Understanding how they are fabricated and used is important for appreciating their performance and limitations. This chapter will, therefore, introduce this class of resonator sensors and describe how these devices can be used for specific detection of biomolecules in solution.

WGM optical resonators exhibit tunability and narrow resonance linewidths, and attain extraordinary optical field intensities that originally led to their use in telecommunications as add-drop filters [62, 63], notch filters [64, 65, 66], and lasers [67]. They have since evolved into valuable tools for probing nonlinear optical phenomena [68, 69] and quantum electrodynamical principles [70]. We are concerned here with the application of WGM optical resonators as chemical sensors, a development that is less than a decade old [5, 6]. In that short time, however, researchers have demonstrated a wide variety of sensing applications. These include, but are not limited to, biochemical assays [71], biomedical assays [72, 73, 74], and molecular biology studies [1, 33]. Their extreme sensitivity (see Chapter 5) in these arenas has generated a great deal of interest in using them to develop analytical and diagnostic instrumentation.

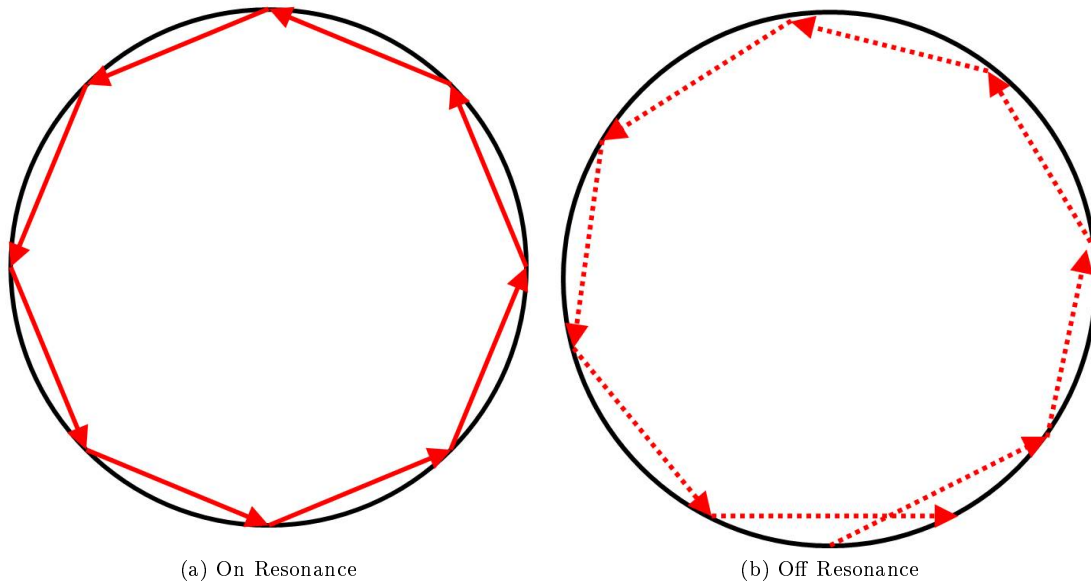


Figure 3.1: Whispering gallery mode resonance in the limit of geometric optics.

3.1 Resonance

Whispering gallery mode resonators derive their name from the path that the resonant light takes as it circulates in the cavity. This path is similar to the one that sound waves took along the curved wall of a circular room studied by Lord Rayleigh [75]. In these whispering galleries, two people standing facing the wall at opposite sides of the room can hear each other even at a whisper. These people would hear not be able to hear each other if either stepped backward toward the center of the room, however. This effect is caused by the smooth, curved walls guiding the sound waves around the periphery of the room with great efficiency. Sound waves taking any other path to the listener are dissipated or scattered en route. WGM optical resonators are dielectric structures capable of trapping light in paths around the periphery similar to those taken by sound waves traveling from one person to another in a whispering gallery. Though Mie [76] and Debye [77] described the resonant eigenfrequencies of dielectric spheres before Lord Rayleigh’s work, the name was not applied to this type of optical resonator until much later.

Light that propagates through a dense material may polarize that medium, depending on how the molecules interact with the time-varying electric and magnetic fields. The permittivity of a material, ϵ_m ,

describes the time delay in the molecular response to the optical fields, and can be expressed in terms of the permittivity of a wave propagating through vacuum, ϵ_0 , and a material-dependent relative permittivity, ϵ_r , i.e., $\epsilon_m = \epsilon_r \epsilon_0$. It is often more convenient to work in terms of the refractive index, whose real part can be expressed as the ratio of the speed of light in a material $v_m(\lambda, T)$ to that in vacuum c . The complex refractive index at temperature T and wavelength λ is defined as

$$n(\lambda, T) = N(\lambda, T) + i\kappa(\lambda, T) = \frac{c}{v_m(\lambda, T)} + i\kappa(\lambda, T). \quad (3.1)$$

The imaginary part of n is related to the loss mechanisms in the material, like absorption or scattering.

The speed of light in the medium is the product of the frequency of the electromagnetic wave, ν , which is independent of the material, and the wavelength in the medium, λ_m . This relationship may be expressed in terms of the speed of light in vacuum, λ_0 , as

$$\lambda_m = \lambda_0 \frac{v_m}{c} = \frac{v_m}{\nu} = \frac{\lambda_0}{n}. \quad (3.2)$$

The fields of optical physics and photonics typically describe light according to its frequency because that value does not vary according to the medium, however the biology community has established as convention the practice of using wavelength to characterize light. Since the present work deals with optical biosensors, I will adhere to the practices of the biology community and refer to the wavelength of light. Equation (3.2) and the expression

$$\Delta\nu = -\Delta\lambda \frac{c}{\lambda^2} \quad (3.3)$$

may be used to convert between frequency or changes in frequency and their equivalents in wavelength-space.

WGM resonators typically have circular cross sections that enable light to be trapped as it propagates near the periphery. This circulating light is confined via total internal reflection at the interface between the resonator and the surrounding medium. Light for which a round trip is equal to an integer number of wavelengths, M , returns to the point it was coupled into the resonator in phase with itself, as illustrated

in Fig. 3.1. Constructive interference occurs under these conditions, allowing the circulating intensity to grow until the rate at which light is coupled into the cavity is balanced by the rate at which it is lost. This phenomenon is referred to as *resonance* and the 3-dimensional electromagnetic field profile that describes the path the resonant light takes is called the *mode*.

For a given resonator, many modes are accessible. A particular mode is characterized by its mode number, which can be approximated as the number of wavelengths within the cavity, M , and by the wavelength required to excite that mode, λ_R . It is apparent from the criteria for resonance

$$2\pi n_{mode} R_{mode} \approx M \lambda_R \quad (3.4)$$

that the resonant wavelength is a function of the refractive index encountered by the mode as well as the radius of the mode, where $R_{mode} \approx R_{res}$ and R_{res} is the radius of the resonator. The free spectral range (FSR) is the wavelength interval that separates a mode of order M and its next-highest order mode ($M+1$). This quantity may be expressed in terms of the resonator size and the excitation wavelength λ as

$$FSR = \frac{\lambda^2}{2\pi n R_{res}}. \quad (3.5)$$

Within one FSR lies a resonant wavelength corresponding to every accessible mode in the device, although each mode may have a different order for a particular interval. Searching for resonant modes in a WGM resonator over an interval longer than one FSR is unnecessary, as one may simply begin finding higher orders of modes that were identified earlier in the search.

3.2 WGM Mode Structure

The electromagnetic field profile for a given WGM resonator is described by the Helmholtz equation

$$\nabla^2 E + \omega^2 \mu \epsilon_m E = 0. \quad (3.6)$$

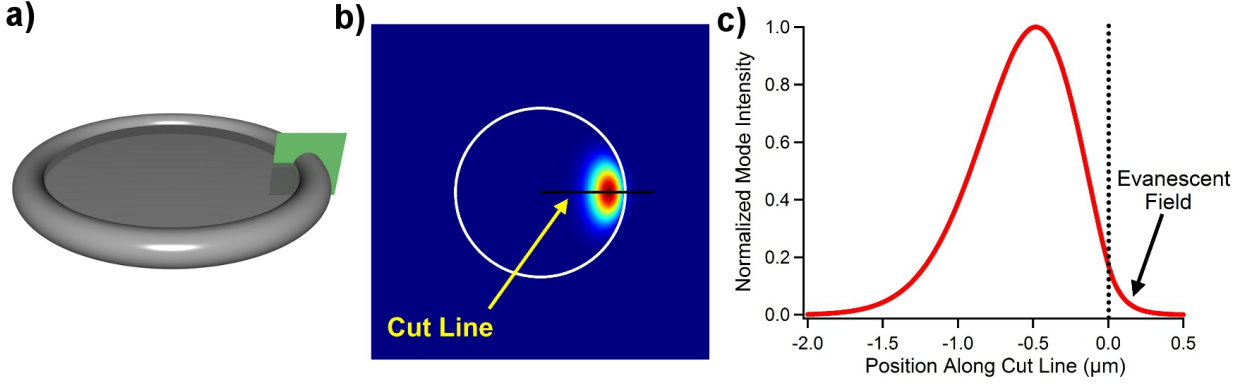


Figure 3.2: (a) A toroidal WGM resonator with a cut plane marked in green. (b) An image of the normalized mode intensity along the cut plane in (a) as calculated using the finite element solver COMSOL Multiphysics. (c) A closer look at the normalized mode structure along the cut line in (b) shows the evanescent field that extends into the water.

Solutions to this equation in spherical and toroidal coordinates are presented (or approximated) elsewhere [78, 79, 80] and describe a feature of WGMs that is critical to their use as sensors. Specifically, the electrical field in the θ -direction (the direction of propagation) can be separated into its contributions in each dimension $E_\theta = \psi_r(r)\psi_\theta(\theta)\psi_\phi(\phi)$. The radial component ψ_r varies with radius r according to

$$\psi_r(r) = \begin{cases} Aj_l(kr) & r < R_{res} \text{ (inside the resonator)} \\ B \exp(-\alpha_{EF}(r - R_{res})) & r \geq R_{Res} \text{ (outside the resonator)} \end{cases} \quad (3.7)$$

where $j_l(kr)$ is a Bessel function of order l (the angular mode number), $k = \omega\sqrt{\mu\epsilon_m}$ is the wavenumber, A and B are constant coefficients, and α_{EF} is the field decay constant. The exponential decay outside of the resonator is the so-called *evanescent field*, and results from total internal reflection.

As can be seen in Figure 3.2, this evanescent field is available to interact with material that either approaches close to or adsorbs onto the resonator surface. One may substitute the effective refractive index, n_{eff} , into the simplified resonance criteria in Eq. (3.4) to more accurately take into account the distribution in optical intensity that spans both the resonator and the surrounding medium. This gives the updated

resonance criteria

$$2\pi n_{eff} R_{mode} \approx M\lambda_R, \quad (3.8)$$

where the effective refractive index is defined as

$$n_{eff} = \frac{\int n(\mathbf{r})E(\mathbf{r})^2 d\mathbf{r}}{\int E(\mathbf{r})^2 d\mathbf{r}}. \quad (3.9)$$

These expressions provide the tools to predict how a resonator will respond when material, like the biomolecules involved in sensing experiments, interacts with the mode.

Any change to n_{eff} or R_{mode} will result in a shift $\Delta\lambda_R$ in the resonant wavelength for a particular mode (i.e., constant M). This relationship was expressed by Vollmer and Arnold [81] as

$$\frac{\Delta\lambda_R}{\lambda_R} = \frac{\Delta n_{eff}}{n_{eff}} + \frac{\Delta R_{mode}}{R_{mode}}. \quad (3.10)$$

Thus, any perturbation of the refractive index or cavity path length, including ones that result from changes in the temperature or composition of the surrounding fluid, will produce a change in λ_R . This is illustrated in Fig. 3.3 by the resonance shift that results from changing the medium surrounding a toroidal WGM resonator from pure water to a common biological buffer solution consisting of sodium phosphate and sodium chloride (also called *phosphate buffered saline*, or PBS). Since the PBS buffer contains solutes with refractive indices greater than that of water, the mode experiences an overall increase in n_{eff} . Replacing the PBS with water again restores the resonator to its previous environment, and the resonant wavelength returns to its original value as expected.

3.3 Quality Factor

The strength of the electromagnetic field available to interact with material that adsorbs to the surface of the resonator is determined by the rate of optical energy coupled into the cavity, P_C , and the rate of loss, P_D . The quality factor Q is the figure of merit used to describe the efficiency with which a resonator contains

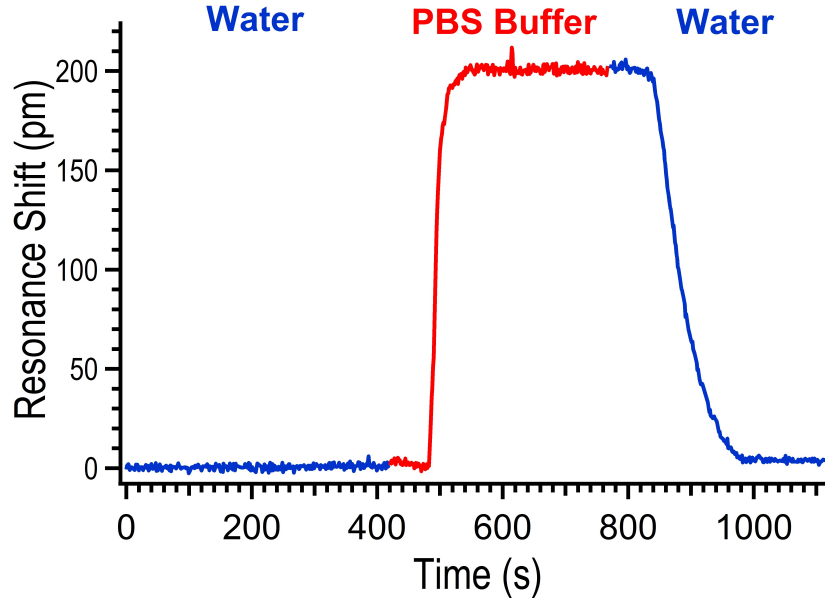


Figure 3.3: Flowing PBS buffer into the flow cell changes the refractive index of the surrounding medium, thereby causing a resonance shift according to Eq. (3.10). This is a basic and non-specific sensing method.

light, and how intense the optical mode is within the cavity. A resonator with a high quality factor loses less light and supports more intense electromagnetic fields than one with a lower Q . The shift in resonant wavelength upon adsorption of material may depend on Q . Though the quality factor can be interpreted in a variety of ways, what follows are the three most common representations of Q .

1. Steady-State Energy Balance

The quality factor may be expressed as the ration of energy stored in the resonator to the energy lost during each optical cycle, where an optical cycle is based on the resonant angular frequency ω_R and $\omega_R = 2\pi\nu_m/\lambda_R$. The total energy in the resonator may be calculated by integrating the energy densities of the electric (\tilde{W}_e) and magnetic (\tilde{W}_m) fields over all positions \mathbf{r} , $W = \int (w_E + w_M) d\mathbf{r}$. At steady-state, the rate of energy lost from the cavity is equal to the rate of energy entering the cavity,

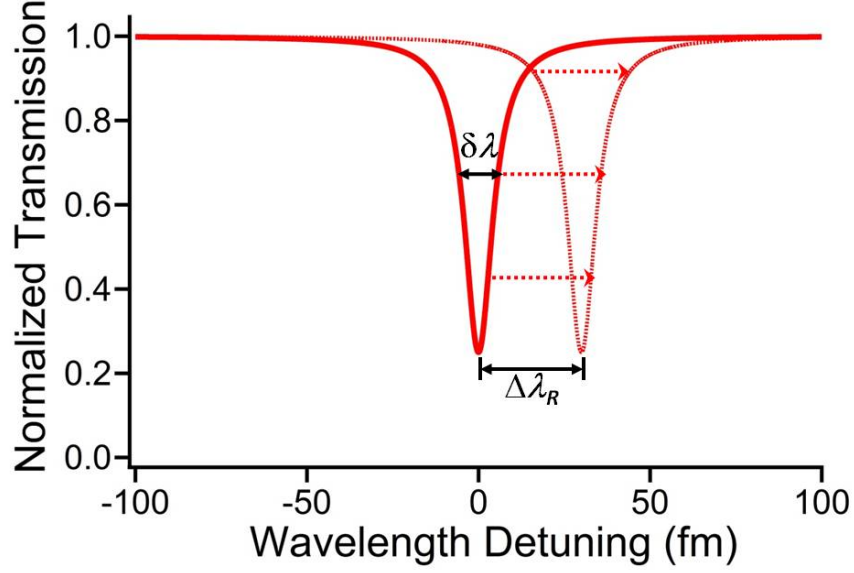


Figure 3.4: Transmission spectra depicting a resonance red-shifting a distance $\Delta\lambda$ in wavelength-space in response to adsorption of protein to the resonator surface. The minimum fractional transmission, along with the total transmission when no light is coupled into the resonator, may be used to calculate the coupled power P_D . The value of Q may also be determined using the observed value of $\delta\lambda_R$ and Eq. (3.12).

leading to the following expression for quality factor:

$$Q = \omega_R \frac{W}{P_D} = \omega_R \frac{W}{P_C}. \quad (3.11)$$

2. Resonance Linewidth

Alternatively, the quality factor may be expressed in terms of the readily measured resonant wavelength (λ_R) and linewidth ($\delta\lambda_R$). Both of these quantities may be determined from a transmission spectrum, like the one in Fig. 3.4, and related to the quality factor using the following simple expression:

$$Q = \frac{\lambda}{\delta\lambda}. \quad (3.12)$$

Note that for an ideal, loss-less resonator, there is an infinite Q because $\delta\lambda_R = 0$.

3. Cavity Ringdown Time

Since the quality factor describes the rate of loss in a material, it is also related to the time required for the light in a cavity to completely dissipate [82]. The instantaneous energy within a resonator is difficult to measure, so this type of cavity ringdown measurement requires monitoring the rate of light leaving the cavity through the optical waveguide previously used to couple light in. A photodetector may be used to measure this leakage light and calculate the quality factor based on an curve fit to that data where the exponential decay constant is the ringdown time τ_{RD} :

$$Q = \omega_R \tau_{RD}. \quad (3.13)$$

These expressions are all equivalent. Moreover, the quality factor can be deconstructed and expressed in terms of the individual loss mechanisms that exist in a resonator. This paradigm was originally introduced by Gorodetsky and colleagues [83] for spherical WGM resonators and expresses the quality factor in a manner similar to how resistors in series contribute to the resistance of a circuit. This expression is

$$\frac{1}{Q_{tot}} = \frac{1}{Q_{mat}} + \frac{1}{Q_{scat}} + \frac{1}{Q_{rad}} + \frac{1}{Q_{ext}}, \quad (3.14)$$

where Q_{mat} refers to the intrinsic material loss, Q_{scat} refers to surface scattering loss, Q_{rad} refers to the tunneling (radiation) loss, and Q_{ext} refers to the losses involved in coupling into external modes. The first three of these terms all involve loss mechanisms *within* the resonator, implying that these mechanisms must be dealt with and minimized in order to fabricate resonators with as high Q values (i.e., electromagnetic field intensities) as possible.

Material Loss

Gorodetsky et al. point out the most significant source of material loss in optical resonators is often absorption of light by the cavity material or the surrounding medium [83]. This loss can be characterized by the absorption decay constant α_{mat} according to

$$Q_{mat} = \frac{2\pi n}{\lambda\alpha_{mat}}. \quad (3.15)$$

This expression can be used to describe how the Q of a cavity will vary with environment within which the measurement is made. For example, the moisture content of air leads to adsorption of water onto a silica resonator, thereby limiting the Q when excited WGMs using light in the near-infrared where water has a high α_{mat} . Lasers in the visible spectrum (e.g., $\lambda = 633$ nm) and their corresponding optical components, which are often more costly than those in the near-infrared range used in telecommunications, are required for WGM optical resonator applications in aqueous environments if ultrahigh quality factors are necessary. The absorption-limited quality factors for resonators in water have been described in detail elsewhere [84].

Scattering Loss

Scattering loss typically occurs as a result of crystal faces in crystalline, anisotropic media or other imperfections where light experiences a discontinuity in refractive index. This includes both internal and surface imperfections that arise from contamination or roughness. Scattering losses may be minimized by choosing amorphous, homogeneous media and taking steps to ensure a smooth surface. Melting amorphous silica has emerged as a strategy to overcome these challenges, found most commonly in the fabrication of microsphere and microtoroidal resonators, and is now sufficiently widespread that scattering losses are rarely the limiting factor in the determination of Q_{tot} . The surface tension of molten silica leads to ultra-smooth surfaces, minimizing both the root mean square (rms) size, σ_{rms} , and length, B , of inhomogeneities. The

scattering-limited quality factor may be expressed as

$$Q_{scat} = \frac{\lambda^2 R_{res}}{\pi^2 \sigma_{rms}^2 B}. \quad (3.16)$$

Radiation Loss

When the path length within a WGM cavity is sufficiently small that the resonant light undergoes few optical cycles during a round trip (i.e. <100), the angle at which that light approaches the interface is steep enough to reduce the efficiency of the total internal reflection responsible for shaping the optical path. Some of this light is lost because it cannot be confined in a path that turns quickly enough. There exists no explicit expression for tunneling loss in a WGM resonator, but the overall radiation loss can be minimized by making using resonators with the largest radii possible for a given application. It appears that for $R_{res} > 30 \mu\text{m}$, absorptive or scattering losses become dominant in silica microspheres [85]. While this provides a lower constraint when selecting a resonator size, the upper bound will come from the free spectral range. Increasing the resonator size will result in an increased mode density in wavelength-space, making it challenging to track the shift of a single resonance due to the overlap of its Lorentzian transmission trough with that of another mode.

3.4 WGM Resonator Fabrication

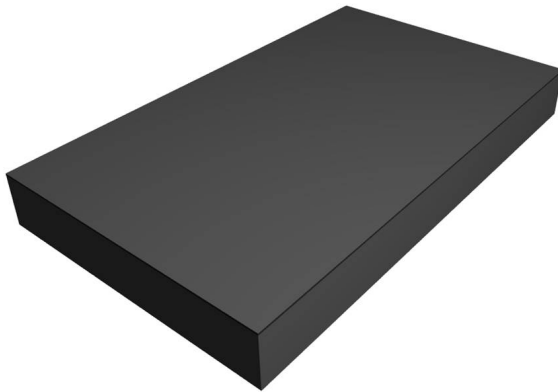
WGM resonators exist in a variety of different geometries, including spheres, cylinders, disks, and toroids. The present work focuses on toroidal resonators, which pose wholly unique fabrication challenges. This process is outlined in Fig. 3.5, and features three steps[82]. The first step is photolithography, which begins with a silicon wafer on which $2 \mu\text{m}$ of thermal oxide has been grown. A photoresist is spun onto the sample and a photomask is used to develop a pattern of circular pads from this layer. These pads protect regions of the silica during the second step, which involves exposure of the entire chip to buffered oxide etchant (BOE), a diluted hydrofluoric acid solution that selectively etches SiO_2 . The photoresist is then washed off of the

sample to reveal a pattern of silica disks on a clean silicon wafer.

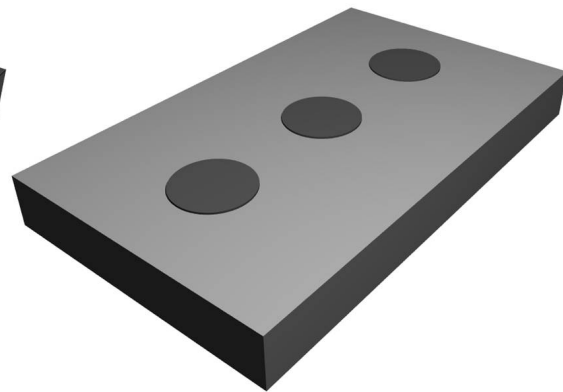
The third step defines microdisk resonators by employing a gas phase XeF_2 etch to isotropically remove *only* the silicon. The glass disks are “undercut,” leaving them resting on silicon pedestals. There are other methods to selectively etch silicon, including concentrated potassium hydroxide, however it etches only along certain crystal faces in the silicon and can produce pedestals that are not round. Figure 3.6 shows one of these pedestals. This XeF_2 etch step is often the slowest of the entire fabrication process. Scaleup is difficult because the etch chamber must efficiently deliver etchant to the sample as evenly as possible (ruling out forced convection) while making sure that the depletion zone formed around one sample does not overlap another sample. The chamber cannot be made too large, however, because it must be pumped down to very low pressures and purged with nitrogen between etchant pulses due to the toxic nature of the etchant and product gases.

The final step of the toroid fabrication process involves melting the edges of the silica microdisk using a focused CO_2 laser putting out $10.6 \mu\text{m}$ normal to the plane of the resonator. This process is often referred to as *reflowing* the disk, and is possible because silica absorbs light $\approx 1000\times$ more efficiently at $10.6 \mu\text{m}$ than the silicon below it. The etching process removes the silicon from beneath some of the disk, ensuring that the absorptive heating of the silica there results in melting. The surface tension of this molten silica at the periphery of the disk drives the symmetric, inward collapse of the structure toward pedestal, which acts as a heat sink preventing the portion of the disk above it from building up sufficient heat to melt. The end result is a silica toroid supported by a silicon pedestal.

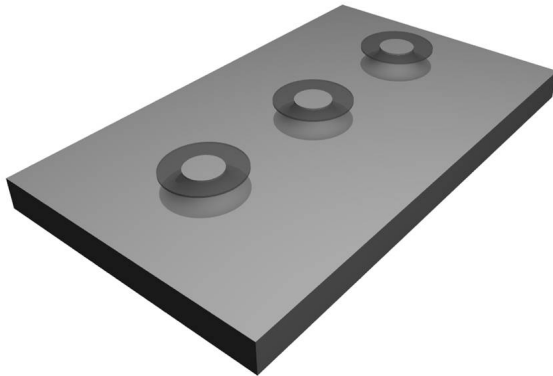
Ultimately, the major and minor radii of the toroid are determined by the diameters of the original disk diameter relative to the pedestal. It is best to manually increase the power of the CO_2 laser, watching the toroid as it forms and stopping when an increase in power fails to produce additional reflow. Extremely high laser powers can generate toroids that are deformed due to the wetting of the silicon pedestal with molten silica. Though these deformed devices will still support WGMs, a great deal of the resonant light will be absorbed by the nearby silicon, resulting in very low quality factors. A helpful rule of thumb to avoid this problem is to stop increasing the power when the separation between the toroid and the pedestal is roughly



(a) Silicon Wafer with Thermal Oxide Layer



(b) Etched Silica Circles



(c) XeF_2 – Etched $\mu\text{DiskResonators}$



(d) Reflowed Toroid Resonators

Figure 3.5: The four-step process to fabricate toroidal WGM resonators on (a) a bare silicon wafer with $2\ \mu\text{m}$ of thermal oxide. (b) Photolithography is used to define a pattern of silica discs through a buffered oxide etch process. (c) The chip is exposed to XeF_2 , an gas that isotropically and selectively etches the silicon from beneath the silica disks. (d) A CO_2 laser at $10.6\ \mu\text{m}$ wavelength light is focused normal to the microdisks, melting the edges and leaving microtoroid resonators on silicon pedestals.

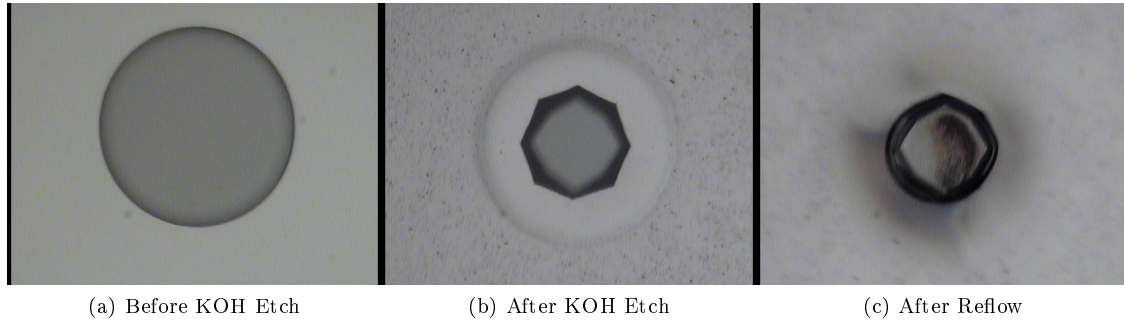


Figure 3.6: Three photographs of a single disk during an experiment to use a KOH etch procedure (10 minute piranha clean followed by a 90 minute exposure to 30 wt% KOH in water) to define a silica disk followed by reflow with a CO₂ laser. The anisotropic nature of the KOH etch produces an off-round pedestal, eliminating any chance of a smooth toroid. Note: field of view in all images is 310 μm wide

equal to the minor diameter of the toroid itself. This optimized laser power may change from one chip to the next as a result of slight nonuniformity of the XeF₂ etch process throughout the etch chamber. The experimental apparatus used for this process is shown in Fig. 3.7.

Microspheres are simpler to make than the toroids and disks described above. Spheres are made by melting the end of a cleaned, stripped optical fiber with either a CO₂ laser setup, as in Fig. 3.7, or a hydrogen flame. In this way, the resonator is really a spherical bulb on the end of a fiber that may be conveniently manipulated. The majority of fiber has an outer diameter of 125 μm , limiting the minimum possible diameter of the resonator. The FSR of such a device is small enough to cause problems resolving single modes during a scan through wavelength space. Smaller spherical resonators that are more useful for biosensing applications may be fabricated by starting with the narrow end of a tapered optical fiber rather than an unaltered piece.

Microcylinder resonators are perhaps the most straightforward to produce, as they require only minor alteration of an optical fiber. In order to remove the polymer jacket of the fiber without scratching the smooth silica surface beneath, I submerge fiber scraps 1 – 2 inches in length into a dichloromethane bath overnight. The polymer absorbs this solvent, swells, and slinks off the fiber like a sock. After a rinse, presents a sufficiently smooth surface that it may support modes with quality factors as high as 2.3×10^7 in water. These results are illustrated in Fig. 3.8. Unlike spherical and toroidal devices, whose geometries include

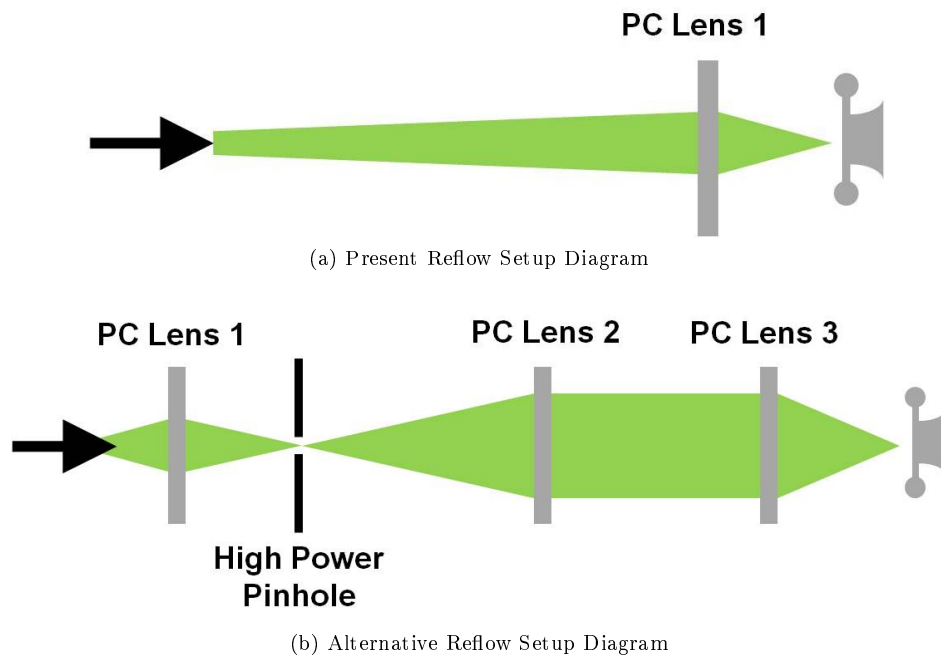


Figure 3.7: Diagrams of experimental reflow apparatus. The black arrow indicates the laser source. Plano-convex (PC) lenses made from ZnSe, which does not absorb light at $10.6 \mu\text{m}$ like silica optics do, are also shown. The alternative setup proposed in (b) may have the advantages of a cleaner beam profile due to both the spatial filter (pinhole) as well as better control over the beam diameter entering the third PC lens.

material interfaces above and below the WGM, cylindrical resonators support many “corkscrew” modes that result in a great deal of loss in the direction normal to the WGM (see Fig. 3.9).

Comparison of toroidal, spherical, and cylindrical resonators reveals inherent advantages and disadvantages of each. Specifically, the minor diameter of a toroid excludes the many non-azimuthal modes that are supported in spherical and cylindrical cavities. The “compression” of the toroidal mode that results from confinement in the axial direction can also make it easier to couple light into the device may be positioned farther from the the cavity than in other geometries while achieving the same coupling efficiency. Work by Spillane also speaks to the relative mode confinement in a sphere and a toroid, pointing out that the optical fields are more intense in a toroid of identical Q due to the vertical compression of the mode compared to a sphere [78]. Spherical and cylindrical resonators, however, do not require access to a cleanroom because they are not made using photolithography. That they are made from relatively inexpensive optical fiber scraps also make these cavity geometries far less expensive than toroids, which require silica-on-silicon wafers. Finally, the process of incorporating a toroidal resonator into a microfluidic cell is far simpler than with spherical and cylindrical devices because they are fabricated on a planar chip that may be attached to the floor of a flow channel. It is clear that all of these features must be taken into account when designing a biomolecular assay based on one of these geometries of WGM optical resonator.

3.5 Coupling Light into WGM Resonators

The task of coupling light into a resonator is one that has been studied thoroughly [86, 87, 88]. This may be accomplished, albeit inefficiently, by simply shining a light onto the resonator. The solutions for a plane wave incident upon a dielectric microsphere are given in detail elsewhere[89]. This Mie scattering pattern predicts that an infinite number of modes exist and all are energy degenerate for an ideal resonator (i.e., no loss). In reality, imperfections lead to some modes existing at a higher energy state than others, a feature that may be exploited to study these quantized states and their interactions as model systems in quantum electrodynamics. In practice, the use of a waveguide leads to far more efficient methods for coupling light

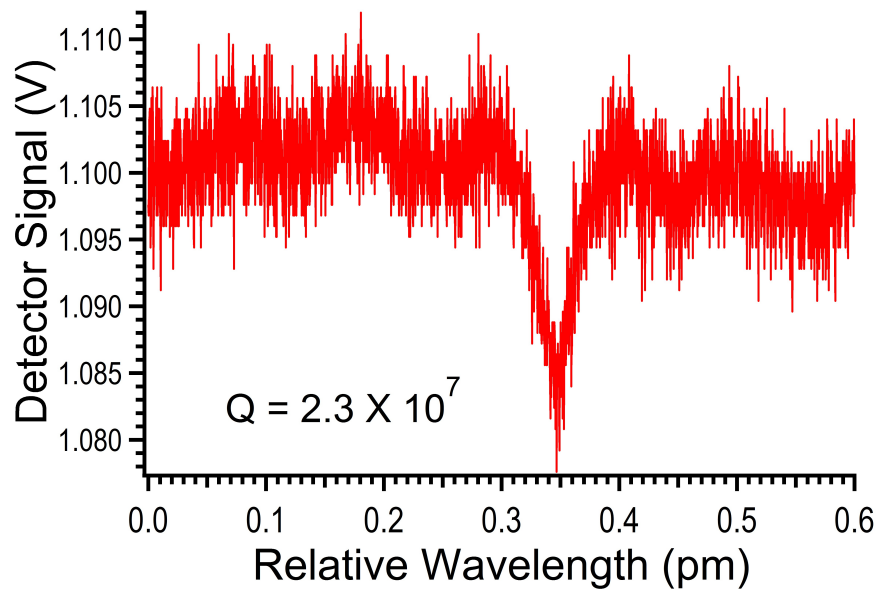


Figure 3.8: Coupling of 633 nm light into a 125 μm diameter optical fiber in water with $Q = 2.3 \times 10^7$

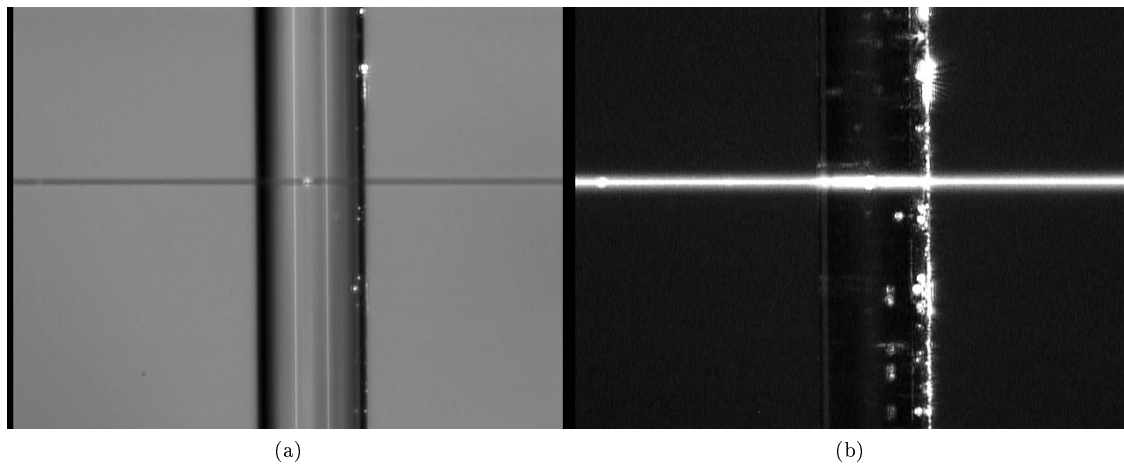


Figure 3.9: Coupling 633 nm light into a microcylindrical WGM resonator. (a) Illumination of the taper and resonator by a bright field, and (b) illumination of the system by only the coupled light. The bright spots in (b) indicate how light is coupled into "corkscrew" modes, reaching parts of the fiber far from the taper and being scattered.

into WGMs. Moreover, waveguide coupling techniques each introduce inherent losses because the waveguide itself may interact with the resonant light and alter the Q via the last term in Eq. (3.14).

Regardless of the method, coupling requires phase matching between the resonant light and incoming light. This means that the overall phase velocities must match, an unlikely event in the case of a free space wave in air or water incident upon a silica resonator. Mismatch leads to a significantly lower coupling efficiency. The fact that light propagates at different velocities in different media implies that one way to achieve phase matching is to simply match the refractive indices of the waveguide and the resonator. This principle has given rise to a number of silica waveguide-based methods for coupling light into silica WGM resonators, which are described in greater detail elsewhere [90, p. 11]. The most common and efficient method involves using a tapered optical fiber waveguide fabricated by pulling the two ends of fiber while it is held over a flame to melt a small section. By creating the tapered section, one provides a small region where the mode leaks out of the fiber radially in an evanescent field. Positioning the resonator in proximity of this field enables coupling with minimal loss.

It is important to use a hydrogen flame to ensure that the taper pulling process does not leave a hydrocarbon film to contaminate the waveguide. While there are some who have pulled tapers often enough that they can simply monitor their thickness using a camera and tell when to stop pulling, the method used in the present work is to monitor the transmission through the taper during the pulling process. As the melted segment thins, it will support a variety of modes that interfere in different ways. The transient signal consequently oscillates with a frequency and amplitude that changes over time to reflect the decreasing number of transmission modes available. The transition to a single-mode regime is marked by the end of oscillations. A single-mode waveguide is required to couple the maximum amount of light possible into a resonator. Multimode waveguides limit this coupling efficiently because only one of the transmission modes, a fraction of the total transmitted optical power, will be phase-matched to the WGM at a time. It is helpful to remember that the single-mode taper diameter is larger in water than air due to the diminished contrast in refractive index. This allows a slightly thicker and more robust single-mode tapered waveguide to be used in biosensing experiments where flow (or collisions between the resonator and taper that result from flow)

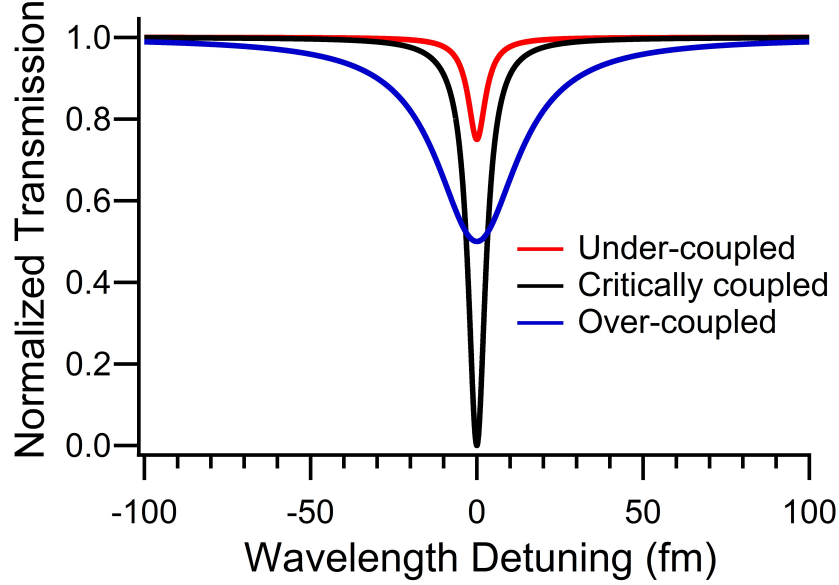


Figure 3.10: Typical transmission profiles illustrating the under-coupled, critically-coupled and over-coupled regimes.

may break the taper.

The overlap of the evanescent field of the waveguide with the resonant mode of the cavity determines how much light is coupled into the device. This coupling efficiency can be tuned through control of the distance separating the waveguide and resonator. Three regimes of coupling behavior are apparent when manipulating that spacing, l_{coup} , which are demonstrated in Fig. 3.10 and described here:

Under-coupled Regime: When $l_{coup} \approx \lambda$, very little of the evanescent wave overlaps the resonant mode of the cavity and P_C is small. Decreasing this gap will couple more light into the resonator until scattering losses due to the presence of the waveguide approach those of the limiting loss mechanism. This is the best regime for determining Q_{tot} so that it reflects the loss mechanisms intrinsic to the resonator.

Critical Coupling: The point at which Q_{ext} becomes the limiting factor in Eq. (3.14) due to scattering of resonant light by the waveguide. Transmission through a perfect, single-mode taper is zero as all light is coupled into the resonator.

Over-coupled Regime: Decreasing the gap between the waveguide and the resonator only decreases the

amount of light getting into the mode because more and more is being lost to scattering by waveguide.

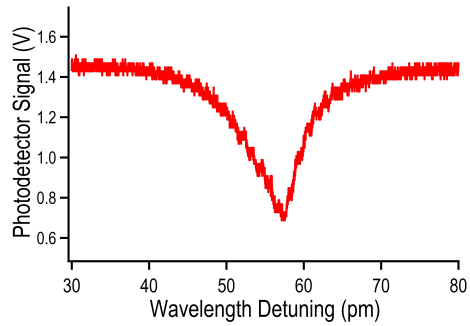
Q_{tot} is dominated by Q_{ext} .

3.6 Nonlinear Effects in WGM Resonators

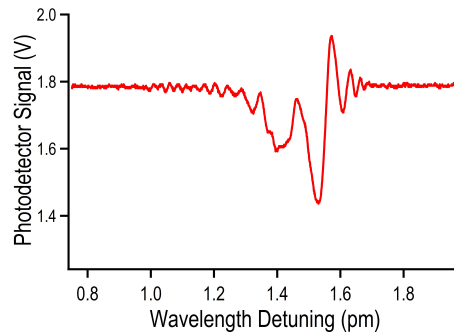
The ability to make resonators with quality factors as high as $Q = 6.3 \times 10^{10}$ [91] while confining the mode into such small volumes makes WGM optical devices perfectly suited to explore nonlinear phenomena in materials. Several well-known second-order effects (i.e., their contribution to the polarization of the medium depends on the electric field magnitude squared, $|\mathbf{E}|^2$), such as second harmonic generation and optical parametric amplification/oscillation may be observed in materials exposed to sufficiently large electric fields. Though fewer in number, some third order phenomena such as the Kerr effect and optical limiting may also be observed. The nonlinear phenomena that play the most prominent role in the present work are discussed in detail in Chapter 5. Fig. 3.11 depicts how these effects manifest themselves in a typical transmission spectrum for a resonant mode.

Of particular importance in studying the WGM biosensor response is the thermo-optical effect. This phenomenon occurs in most materials and applies to how the refractive index defined in Eq. (3.1) varies with temperature according to the thermo-optical coefficient $\frac{dn}{dT}$. The small amount of optical energy absorbed by the silica in a resonator is dissipated as heat because no radiative relaxation (e.g., fluorescence) is available to it. For silica, $\frac{dn}{dT} = 1.3 \times 10^{-5} \text{ K}^{-1}$ and warming produces an increase in the refractive index. Eq. (3.10) suggests that any increase in the effective refractive index n_{eff} will produce a red shift ($\Delta\lambda > 0$). Transmission spectra are transient measurements collected as the wavelength is scanned and light is coupled into the resonator.

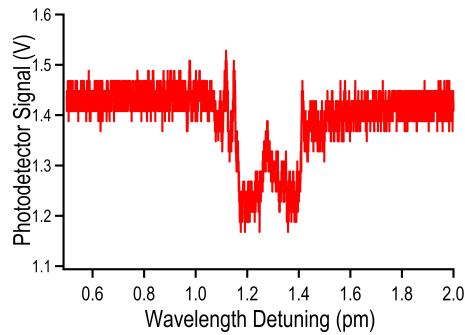
As the instantaneous output of the scanned laser approaches the resonant wavelength λ_R and light is coupled into the mode, the heat generated by absorption increases the cavity temperature and the resonant wavelength shifts. The transmission curve changes from a symmetrical Lorentzian shape to an asymmetrical sharkfin-like shape, with an artificially wide trough observed while $\frac{d\lambda}{dt} > 0$ and an artificially narrow one



(a) Thermal Broadening



(b) Opto-mechanical Oscillations



(c) Resonance Splitting

Figure 3.11: Nonlinear effects observed while coupling into WGM resonators. (a) Asymmetrical transmission trough for a $150 \mu\text{m}$ microdisk excited with 1310 nm light. (b) Opto-mechanical oscillations as the momentum of propagating light excites mechanical vibration modes in a microtoroidal resonator excited with 1540 nm light. (c) A split resonance peak as backscattering in the cavity can break the degeneracy of counter propagating modes in a microtoroidal resonator excited with 1310 nm light

when $\frac{d\lambda}{dt} < 0$. This effect is demonstrated in Fig. 3.11a. The thermo-optical effect is greater detail in Chapter 5. This thermal broadening effect can be managed by using low coupled power, but eliminating absorption by the bulk materials is impossible for near-infrared light in water or visible light in silica.

Another nonlinear effect involves mechanical feedback that results from the momentum of the resonant light [92, 93, 94]. Circulating photons can apply enough force at certain frequencies to excite vibrational modes in microdisks and microtoroids supported on silicon pedestals. Since coupling into the resonator is sensitive to the relative position of the cavity and the waveguide, any mechanical oscillations directly effect the coupling. Fig. 3.11b illustrates this phenomena and how coupling more light during the wavelength sweep increases the amplitude of mechanical oscillation and distorts the transmission trough.

A third nonlinear phenomena that appears often when working with high- Q WGM optical resonators ($Q > 10^7$) involves what are called split peaks. When inhomogeneities in or on the resonator are efficient enough at scattering light backwards, the counter-propagating mode is excited. The two modes have a different resonant wavelengths because their path lengths vary slightly due to the backscattering, resulting in a transmission profile that features two local minima rather than the single Lorentzian trough observed in the absence of this effect (see Fig. 3.11c). Since the magnitude of the backscattered wave is determined by the size and number of inhomogeneities present, the mode splitting can be used to report the quantity of material as well as the nature (e.g., size, refractive index, geometry) of that inhomogeneity. This effect has been described [95] and demonstrated [96] elsewhere. This phenomena is only observed in sufficiently high-quality resonators because there is a threshold circulating power required to sustain resonance in the counter-propagating direction, and those powers are attainable with quality factors of $Q > 10^7$.

3.7 Sensing with WGM Resonators

WGM sensing experiments are carried out by monitoring the resonant wavelength as analyte solution is introduced to the sensor. This process involves enclosing the resonator and waveguide inside a flow cell while scanning through wavelength space and capturing transmission spectra. The apparatus used for this

measurement is shown in Fig. 3.12, and the flow cell configuration used for the experiments in the present work is depicted in Fig. 3.13. The flow cell is constructed on the end of a stainless steel sample holder that may be fixed to a positioning system. Manipulation of the gap between the resonator and the waveguide is performed by keeping the tapered optical fiber waveguide immobile while moving the resonator and the flow cell into which it is incorporated. A range of motion of roughly 25 mm is usually required to test multiple resonators defined on a single chip in search of the mode with the highest Q , but great precision is also required to control the light coupled into the device. This difficult combination is achieved by attaching a 3-dimensional piezo positioning system (range of motion 100 μm) to a 3-dimensional translation stage (range of motion 25 mm).

Cameras with microscope objectives are positioned to give a top and side view of the waveguide and resonator, with lamp light coupled down the optical axis of these camera systems to provide sufficient illumination. The top view provides useful feedback during the positioning of the resonator, but ultimately the power coupled into the cavity provides the most precise information about how close the device is to the waveguide. The relative coupled power as well as the instantaneous λ_R may be read from the transmission spectrum data sent from a low-noise photodetector to an oscilloscope. The side view camera enables the planar alignment of the waveguide and the resonator, which is extremely important for toroidal devices because they do not support non-equatorial modes. This entire apparatus, with exception to the oscilloscope, is enclosed in a box to limit environmental effects on the system. Fig. 3.14 shows a top view image of a toroid and tapered optical fiber waveguide in far-field illumination as well as one illuminated only by the light coupled into the device. Notice the striation-like defects in the toroid visible in Fig. 3.14b.

The external cavity laser is scanned by sending it a customized triangular function from a waveform generator. The oscilloscope that receives the data from the photodetector reports the total power to the diode as a function of time, which may then be converted to wavelength with knowledge of the triangular waveform characteristics. Programs were written in both LabVIEW and Igor to be run on a computer in order to query and retrieve data from the oscilloscope. The scanning of the excitation laser underscores the transient nature of this measure. More detail about the experimental method behind WGM optical biosensor

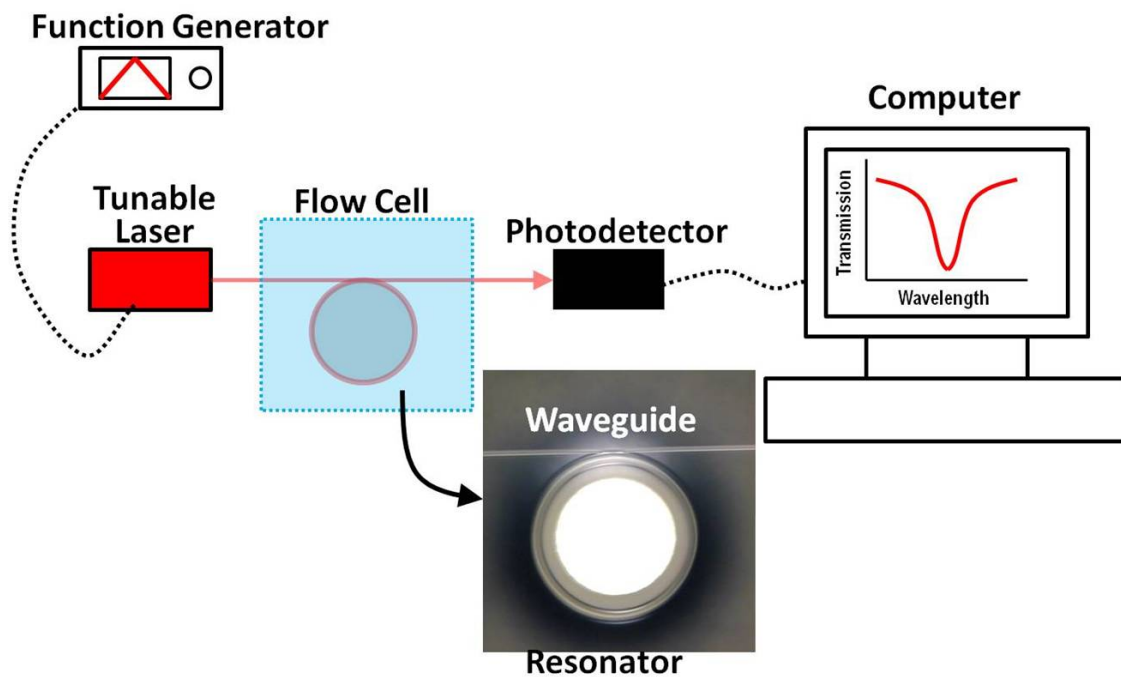


Figure 3.12: The WGM sensing experimental apparatus, featuring a tunable laser, tapered optical fiber waveguide, resonator, detector and data capture/processing computer. A function generator is used to sweep linearly through wavelength space so that a transmission spectrum may be used to locate the center of the resonance peak or determine the Q of the resonance.

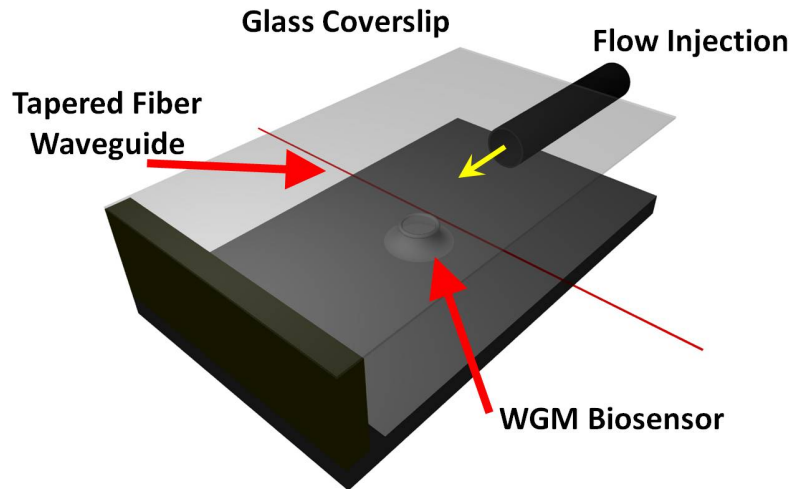


Figure 3.13: The flow cell used in WGM biosensor experiments, shown with a microtoroidal resonator and tapered optical fiber.

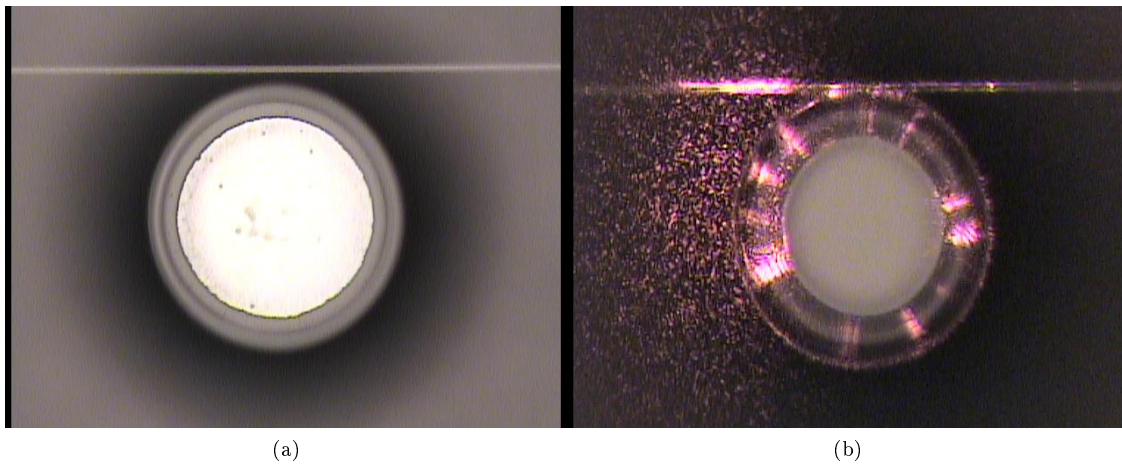


Figure 3.14: Using a tapered optical fiber waveguide to couple light into a toroid. (a) A view showing the two in proximity to one another. (b) A low-quality toroidal WGM resonator ($Q \approx 10^2$) scattering light out of the cavity.

experiments as well as a thorough discussion of the role that transient behavior plays in the interpretation of these results is included in Chapter 5.

The processing of data involves determining the location of the resonance based on each captured transmission spectrum. As discussed above, nonlinear effects like thermal broadening can complicate the process of finding the resonant wavelength from this spectrum because it changes with the temperature of the resonator. In this case, the minimum may be an effective measure of the resonance location, assuming that the material that adsorbs to the sensor during the experiment does not significantly perturb the shape of that trough. For low- P_C conditions, however, the trough will be well described by a Lorentzian function that may be determined through curve fitting. A study of this data processing step revealed that a curve fit, though time consuming considering the typical time resolution of the measurement that generates a single scan for every 0.5–1 s, does a better job of preserving small features in the data than applying a smoothing function and determining the minimum of the curve.